Causal Dispersive Plasma-Inversion Point-Ahead Tracking and Doubly-Stochastic Cox–Bessel Demodulation for Interplanetary Optical–RF Satellite Communications

Sai Thrinay Potta, *Member, IEEE*

***Abstract*—Near Superior Solar Conjunction ($\alpha_{\text{SEP}} \leq 5^\circ$), coronal electron wedges ($\nabla_\perp$STEC), temporal plasma drift (dSTEC$/dt$), and the 1517 s Round-Trip Light Time (RTLT at $D = 1.52$ AU) degrade Earth-referenced point-ahead tracking, while daytime scintillation and residual slot drift induce doubly-stochastic Cox photon bunching that saturates linear Poisson log-likelihood ratios (LLRs). This letter presents a causal two-node optical–RF transceiver requiring no ground laser beacon. Onboard the spacecraft, Deep Space Network (DSN) X/Ka-band uplinks are inverted via Lorentz–Appleton–Hartree group–phase duality, Gauss–Markov Best Linear Unbiased Estimation (BLUE), and radial Abel advection to compensate coronal orbit-determination bias. At the Earth receiver, a soft-posterior timing error detector (TED) with 1D Kalman tracking and a 3-slot Negative-Binomial co-spill demodulator (Theorem 1) reduce pointing error from 3.409 to 0.763 μrad, slot drift by $11.4\times$, and coded Frame Error Rate (FER) by $9.3\times$ ($64.2\times$ under 960-bit SCPPM), sustaining 36.97 Mbps at Mars conjunction ($D = 1.52$ AU, $\alpha_{\text{SEP}} = 2.5^\circ$).**

***Index Terms*—Deep-space optical communications, point-ahead tracking, solar corona, M-PPM, Cox process, soft demodulation.**

I. Introduction

DEEP-SPACE optical links such as the Lunar Laser Communication Demonstration (LLCD) [1] and Deep Space Optical Communications (DSOC) [2] employ 1550 nm M-ary Pulse-Position Modulation (M-PPM) [3]–[5] with Superconducting Nanowire Single-Photon Detector (SNSPD) arrays [6]. However, operating near Superior Solar Conjunction [7]–[9] over $D \in [0.52, 2.67]$ AU and Sun–Earth–Probe angles $\alpha_{\text{SEP}} \in [1.0^\circ, 5.0^\circ]$ introduces severe tracking and detection bottlenecks.

First, narrow optical beams ($w_0 = 5.07$ μrad for a $D_{\text{tx}} = 0.22$ m aperture) require steering ahead by $\theta_{\text{PAA}} = 2v_\perp/c \approx 232.16$ μrad [10], [11]. At $D = 1.52$ AU (OWLT $= 758.5$ s, RTLT $= 1517.0$ s), solar wind advects coronal structures across the ray path with coherence time $\tau_{\text{cor}} \approx 420$ s, rendering Earth-loop pointing updates stale ($\exp(-\text{RTLT}/\tau_{\text{cor}}) = 0.027$), while 5 kW uplink beacons suffer atmospheric tilt wander and daytime background glare [2]. Simultaneously, Slant Total Electron Content (STEC $= \int N_e(s)\, ds$) gradients $\nabla_\perp$STEC and drift $\dot{S} \triangleq d\text{STEC}/dt$ bias single-band ΔDOR and Doppler Orbit Determination (OD) [8], [12], inducing 3.409 μrad pointing RMSE (3.00 dB loss).

The author is with SRH University of Applied Sciences, Berlin, Germany (e-mail: thrinaypotta@gmail.com; thrinay@ieee.org).

TABLE I
Nominal Deep-Space Link and Transceiver Parameters

Parameter	Symbol	Nominal Value
Link distance & SEP angle	D, α_{SEP}	1.52 AU, 2.5° ($9.38\, R_\odot$)
One-way / round-trip light time	OWLT, RTLT	758.5 s, 1517.0 s
DSN X / Ka uplink frequencies	$f_{X,\text{up}}, f_{Ka,\text{up}}$	$7.18, 34.35$ GHz
Solar wind & orbital angle	$\bar{v}_{\text{eff},\perp}, \cos\psi_{\text{orb}}$	385.2 km/s, 1.0
OD & LPF parameters	$f_{\text{nav}}, G_{\text{DDOR}}, K_{\text{OD}}, \tau_{\text{LP}}$	11.8 GHz, 18.5, 38 km, 600 s
Spacecraft optical TX	$\lambda_{\text{opt}}, D_{\text{tx}}, P_{\text{tx}}$	1550 nm, 0.22 m, 4.5 W
Modulation & slot width	$M, T_{\text{slot}}, T_{\text{sym}}$	64-PPM, 1.0, 80.0 ns
Earth RX aperture & SNSPD	$D_{\text{rx,eff}}, N_{\text{pix}}, \tau_{\text{dead}}$	6×5.1 m, 32 pix, 10 ns
Signal & background counts	$n_{s,0}, n_b$	4.588 ph/pulse, 0.0566 ph/slot
Kalman timing noise & TDC	$Q_b, \Delta t_{\text{TDC}}$	6.4×10^{-5} slots^2, 15.625 ps

Second, at the ground station, although cold-plasma refractivity scales as λ^2 and leaves the 1550 nm beam free of coronal scintillation, daytime atmospheric turbulence [15], K/F-corona background glare [13], and $N_{\text{pix}} = 32$ SNSPD dead-time blocking ($\tau_{\text{dead}} = 10.0\, T_{\text{slot}}$) induce super-Poissonian photon bunching and inter-slot spill [14]. Standard CCSDS linear Poisson LLRs ($\ell_m \propto k_m$) [3], [5] assign excessive weight to bunched noise surges, causing decoder saturation (FER $= 1.000$).

To overcome both bottlenecks without ground beacons, this letter presents: 1) a causal onboard point-ahead tracker that fuses dual-band DSN X/Ka uplinks via Gauss–Markov Best Linear Unbiased Estimation (BLUE) and radial Abel advection; and 2) a ground 3-slot Negative-Binomial co-spill demodulator (Theorem 1) coupled with a soft-posterior 1D Kalman timing loop.

II. System Model and Two-Node Channel Physics

Consider a deep-space link over heliocentric range D at solar elongation α_{SEP} (Table I). Along the ray $s \in [0, D]$, the solar impact parameter is $R_0 = D_\oplus \sin\alpha_{\text{SEP}}$ at $s_c = D_\oplus \cos\alpha_{\text{SEP}} \approx 1.00$ AU. The coronal electron density $N_e(r)$ at $\tilde{r} \triangleq r/R_\odot$ follows the three-term Leblanc profile [7]:

$$N_e(r) = c_1\tilde{r}^{-2.3} + c_2\tilde{r}^{-6} + c_3\tilde{r}^{-16} + \delta N_e(\mathbf{r}, t), \qquad (1)$$

with synoptic coefficients $(c_1, c_2, c_3) = (3.3 \times 10^{11}, 4.1 \times 10^{12}, 8.0\times10^{13})$ m^{-3} and 8% Kolmogorov boiling δN_e ($\tau_{\text{cor}} \approx 420$ s).

A. Node 1 (Spacecraft at t_{tx}): Relativistic Point-Ahead

At transmission epoch t_{tx}, the spacecraft receives the coherent DSN X/Ka uplink along impact parameter $R_{0,\text{up}} =$

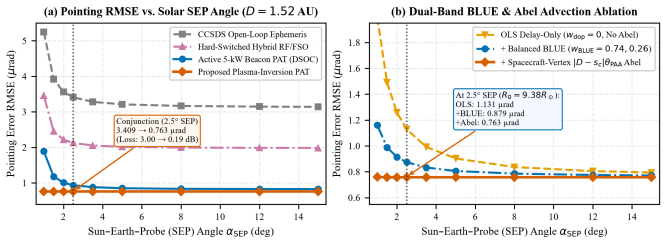


Fig. 1. Causal onboard point-ahead tracking at $D = 1.52$ AU: (a) Pointing RMSE vs. α_{SEP} ($3.409 \rightarrow 0.763$ μrad at 2.5°); (b) OLS group-delay slope vs. BLUE $(0.74, 0.26)$ and Abel radial advection.

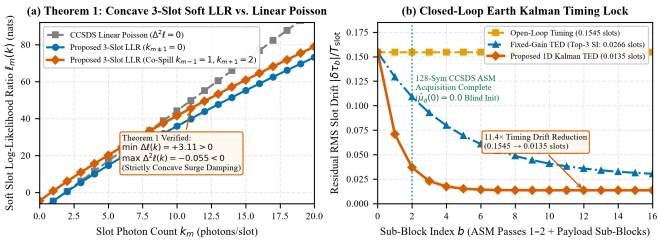


Fig. 2. Theorem 1 and closed-loop Kalman timing at 1.52 AU, 2.5°: (a) Concave 3-slot soft LLR $\ell_m(k)$ vs. linear Poisson LLR; (b) Sub-block RMS slot drift ($0.1545 \rightarrow 0.0135$ slots).

$R_0 - \Delta R_{0,\text{PAA}}$ and steers its 1550 nm and 31.95 GHz downlink beams ahead by the relativistic point-ahead angle [10], [11]:

$$\theta_{\text{PAA}}(t_{\text{tx}}) = \frac{2v_\perp(t_{\text{tx}})}{c\sqrt{1-\beta^2}} - \frac{2v_\perp v_{\text{rad}}}{c^2} + \theta_{\text{PN}}(R_0, D), \quad (2)$$

where $\beta = v/c$ and $|\theta_{\text{PN}}| \leq 5 \times 10^{-4}$ μrad collects post-Newtonian gravitational and Shapiro terms. Because the uplink and downlink rays intersect at the spacecraft vertex ($s = D$) while separated by $v_\perp \text{RTLT} = D\theta_{\text{PAA}}$ at Earth ($s = 0$), similar triangles yield a radial offset $\Delta R_{0,\text{PAA}} = |D - s_c|\theta_{\text{PAA}} \cos\psi_{\text{orb}} = 18,090$ km at the coronal screen ($s = s_c$), corresponding to an advection lag $\Delta t_{\text{adv}} = \Delta R_{0,\text{PAA}}/\bar{v}_{\text{eff},\perp} = 47.0$ s $\ll \tau_{\text{cor}}$.

B. Node 2 (Earth Receiver at $t_{rx} = t_{tx} + \text{OWLT}$): Cox Channel

At reception epoch t_{rx}, the 1550 nm M-PPM pulse arrives at the $N_{\text{pix}} = 32$ WSi SNSPD array [6]. Under Gamma–Gamma atmospheric scintillation $I \sim \text{GG}(\alpha, \beta)$ [15], residual pointing error $\theta_{\text{err}}(t)$, and fractional clock offset $\delta\tau_b \in (-0.5, 0.5)$ slots, pulse energy spills across the three adjacent slots $\delta \in \{-1, 0, +1\}$ around the transmitted slot $m^\star$ with ratios η_δ ($\sum_{\delta=-1}^{+1} \eta_\delta = 1$). Let $r_\delta = \eta_\delta n_{s,0} I \exp(-2\theta_{\text{err}}^2/w_0^2) + n_b$ denote the incident photon rate in slot $m^\star + \delta$, where n_b sums K/F-corona glare [13] and detector dark counts. Accounting for sequential dead-time blocking ($\tau_{\text{dead}} = 10.0\, T_{\text{slot}}$) across N_{pix} nanowires, the effective detected slot rate is

$$\tilde{\lambda}_{m^\star+\delta} = \frac{r_\delta}{1 + \ell_{\text{bg}} + (r_\delta + \chi_{\text{prev},\delta})/N_{\text{pix}}}, \quad (3)$$

where $\ell_{\text{bg}} = \tau_{\text{dead}} n_b/(N_{\text{pix}} T_{\text{slot}})$ is the steady background blocking fraction and $\chi_{\text{prev},\delta}$ captures the carry-over dead-time shadow from the preceding pulse slots.

III. Proposed Tracking and Demodulation Architecture

A. Causal Dual-Band Plasma-Inversion Point-Ahead Tracking

Under cold-plasma dispersion $n_p(f) \approx 1 - \mathcal{K}N_e/f^2$ ($\mathcal{K} = 40.308$ m^{3}s^{-2}), the group delay $\tau_g(f) = \tau_{\text{vac}} + (\mathcal{K}/cf^2)S$ and phase delay $\tilde{\tau}_\phi(f) = \tau_{\text{vac}} - (\mathcal{K}/cf^2)S + N_{\text{amb}}/f$ ($S \triangleq$ STEC) satisfy $v_g(f)v_\phi(f) = c^2$. Their cycle-slip-free derivative average $\frac{1}{2}[\dot{\tau}_g(f) + \dot{\tilde{\tau}}_\phi(f)] = \dot{\tau}_{\text{vac}}$ cancels $1/f^2$ plasma drift, while dual-band X/Ka ranging $\Delta\tau_{g,X,Ka} = \Gamma_{X,Ka}\bar{S}_{\text{up}}$ measures synoptic $\bar{S}_{\text{up}}$, and dual-band carrier Doppler $\Delta f_{D,\text{up}} = f_D(f_{X,\text{up}}) - (f_{X,\text{up}}/f_{Ka,\text{up}})f_D(f_{Ka,\text{up}}) = S_{f,\text{up}}\dot{S}_{\text{up}}$ isolates the instantaneous drift rate $\dot{S}_{\text{up}}$.

Over an $N_{\text{ep}} = 16$ epoch ($\Delta t_{\text{ep}} = 0.5$ s, 8.0 s) onboard filter window, let $\hat{\dot{S}}_{\text{OLS}}$ and $\hat{\dot{S}}_{\text{Dop}}$ denote the group-delay Ordinary Least Squares (OLS) slope and dual-band phase-rate estimators, with error variances σ^2_{OLS}, σ^2_{Dop}, and common-mode boiling covariance σ_{cov}. The Gauss–Markov BLUE fusion weight is

$$w^\star_{\text{Dop}} = \frac{\sigma^2_{\text{OLS}} - \sigma_{\text{cov}}}{\sigma^2_{\text{OLS}} + \sigma^2_{\text{Dop}} - 2\sigma_{\text{cov}}} \approx 0.74, \quad (4)$$

giving $\hat{\dot{S}}_{\text{up,BLUE}} = w^\star_{\text{Dop}}\hat{\dot{S}}_{\text{Dop}} + (1 - w^\star_{\text{Dop}})\hat{\dot{S}}_{\text{OLS}}$. Integrating (1) along the line of sight via the Euler–Beta Abel integral yields power-law terms $S_\ell(R_0) \propto R_0^{1-p_\ell}$ ($p_\ell \in \{2.3, 6, 16\}$) with transverse gradient $|\nabla_\perp \bar{S}(R_0)| = [(\bar{p}(R_0) - 1)/R_0]\bar{S}(R_0)$ and logarithmic curvature $p_{\text{eff}}(R_0) = -R_0 \partial \ln|\nabla_\perp \bar{S}|/\partial R_0$. Mapping the first-order IIR low-pass filtered drift $\hat{\dot{S}}_{\text{up,LPF}}$ ($\tau_{\text{LP}} = 600$ s) to the uplink gradient $\nabla_\perp \hat{S}_{\text{up}} = -\bar{v}^{-1}_{\text{eff},\perp}\hat{\dot{S}}_{\text{up,BLUE}}\hat{\mathbf{u}}_r$ ($\bar{v}_{\text{eff},\perp} = |\hat{\dot{S}}_{\text{up,LPF}}|R_0/[(\bar{p}(R_0) - 1)\bar{S}_{\text{up}}]$) and applying first-order radial Taylor advection across $\Delta R_{0,\text{PAA}}$ yields the causal downlink gradient at t_{tx}:

$$\nabla_\perp \hat{S}_{\text{down}} = \nabla_\perp \hat{S}_{\text{up}} \left[1 - \frac{p_{\text{eff}}(R_0)}{R_0}\Delta R_{0,\text{PAA}}\right]. \quad (5)$$

Subtracting the resulting single-band ($f_{\text{nav}} = 11.8$ GHz) coronal ΔDOR ($G_{\text{DDOR}} = \partial\theta_{\text{OD}}/\partial\theta_{\text{DDOR}} = 18.5$) and two-way Doppler ($K_{\text{OD}} = (c/2)\partial\theta_{\text{OD}}/\partial\dot{\rho} = 38$ km) OD bias $\hat{b}_{\text{cor}}(t_{\text{tx}}) = (\mathcal{K}/f^2_{\text{nav}})[G_{\text{DDOR}}|\nabla_\perp \hat{S}_{\text{down}}| + (2K_{\text{OD}}/c)\hat{\dot{S}}_{\text{up,LPF}}]$ directly onboard at t_{tx} reduces conjunction pointing RMSE from 3.409 to 0.763 μrad (Fig. 1).

B. 3-Slot Soft Demodulation and Kalman Slot Synchronization

At the Earth receiver, each 320-symbol (25.60 μs) sub-block b yields slot photon counts $\mathbf{k}_i = [k_{i,0}, \ldots, k_{i,M-1}]^T \in \mathbb{Z}^M_{\geq 0}$. To estimate channel moments blindly without order-statistic bias, the receiver masks the 3-slot cyclic window $\mathcal{W}_i = \{\hat{m}_i - 1, \hat{m}_i, \hat{m}_i + 1\} \pmod M$ around each symbol peak $\hat{m}_i = \arg\max_m k_{i,m}$. The $M - 3$ unmasked background slots provide the background mean $\hat{n}_b$ and clumping parameter $\hat{\kappa}_0 = \hat{n}_b^2/(\text{Var}[k_{\text{bg}}] - \hat{n}_b)$. From the symbol sum $K_i = \sum_{m=0}^{M-1} k_{i,m}$ and 3-slot window sum $K_{i,\mathcal{W}} = \sum_{\delta=-1}^{+1} k_{i,(\hat{m}_i+\delta) \bmod M}$, the receiver estimates the mean signal count $\hat{n}_s = \max(\bar{K} - M\hat{n}_b, 0.05)$, the normalized 3-slot spill weights $\hat{\eta}_\delta = g_\delta/\sum_{\nu=-1}^{+1} g_\nu$ ($g_\delta = \max(\bar{k}_{\hat{m}+\delta} - \hat{n}_b, 0.01)$), and the dead-time-decompressed Mandel scintillation index $\hat{\text{SI}}_{\text{tot}} = 0.55\hat{\text{SI}}_{\text{obs}} + 0.45\text{SI}_{\text{prior}}$ (fusing the 3-slot empirical

TABLE II
PERFORMANCE COMPARISON (MEAN ± SE) AT SUPERIOR SOLAR CONJUNCTION ($D = 1.52$ AU, $\alpha_{\text{SEP}} = 2.5^\circ$, $R_0 = 9.38\,R_\odot$, 64-PPM)

System Configuration	Pointing RMSE (μrad ± SE)	Loss (dB)	Slot Drift (slots ±SE)	Uncoded SER (raw)	Coded BER ([16, 8, 5] QR)	Coded FER ([16, 8, 5] ± SE)	SCPPM FER (960-bit)	Goodput (Mbps ± SE)	CPU Time (μs/block)
1. CCSDS 141.0-B-1 Static Poisson [3], [5]	3.409 ± 0.003	3.00	0.3914 ± 0.0034	0.6534	0.25334	1.0000 ± 0.0000	1.0000 ± 0.0000	0.35 ± 0.00	5.18
2. Active 5 kW Ground Beacon PAT [2]	0.934 ± 0.004	0.27	0.2283 ± 0.0034	0.2657	0.02824	0.5083 ± 0.0409	0.3717 ± 0.0495	18.78 ± 1.53	5.35
3. Hard-Switched Hybrid RF/FSO [9]	2.124 ± 0.005	1.28	0.2745 ± 0.0034	0.4051	0.08985	0.8942 ± 0.0177	0.8608 ± 0.0190	0.25 ± 0.00	4.20
4. Proposed Causal PAT Only (Open-Loop)	$\mathbf{0.763 \pm 0.006}$	**0.19**	0.1545 ± 0.0162	0.2006	0.01057	0.2167 ± 0.0580	0.1092 ± 0.0482	29.72 ± 2.17	5.20
5. **Proposed Combined PAT + 3-Slot Receiver**	$\mathbf{0.763 \pm 0.006}$	**0.19**	$\mathbf{0.0135 \pm 0.0020}$	**0.1242**	**0.00099**	$\mathbf{0.0233 \pm 0.0040}$	$\mathbf{0.0017 \pm 0.0004}$	$\mathbf{36.97 \pm 0.15}$	**23.83**

Mandel index $\hat{\text{SI}}_{\text{obs}} = (\text{Var}[\tilde{K}_{i,\mathcal{W}}] - \bar{\tilde{K}}_{i,\mathcal{W}} - 3\tilde{n}_b^2/\hat{\kappa}_0)/(\bar{\tilde{K}}_{i,\mathcal{W}} - 3\tilde{n}_b)^2 = 0.169$, where $\tilde{K}_{i,\mathcal{W}}$ and $\tilde{n}_b$ invert (3), with the Gamma–Gamma Rytov prior SI_{prior} [15]).

Conditioning a Poisson slot count on Gamma-distributed pulse intensity yields a Negative-Binomial marginal with effective dispersion $\tilde{\kappa}_{1,\delta} = \hat{\kappa}_0[1 + \rho_\delta/(1+\xi)]$, where $\rho_\delta = \hat{\eta}_\delta \hat{n}_s/\hat{n}_b$ and $\xi = \hat{\kappa}_0 \hat{\text{SI}}_{\text{tot}}$. Incorporating adjacent-slot co-spill correlation $\gamma_{\text{co}} = \gamma_0 \hat{\text{SI}}_{\text{tot}}/(1 + \hat{\text{SI}}_{\text{tot}})$ ($\gamma_0 = 0.42$) yields the 3-slot soft demodulator characterized below.

Theorem 1 (Strict Monotonicity and Strict Concavity of the 3-Slot Soft LLR)**.** *For any slot count vector $\mathbf{k}_i \in \mathbb{Z}_{\geq 0}^M$ with $\hat{n}_s, \hat{n}_b, \hat{\kappa}_0, \hat{\text{SI}}_{\text{tot}}, \hat{\eta}_0 > 0$, $\hat{\eta}_{\pm 1} \geq 0$, and $k_\delta \triangleq k_{i,(m+\delta) \bmod M}$, define the 3-slot soft log-likelihood ratio for candidate slot m as*

$$\ell_m(\mathbf{k}_i) = \sum_{\delta=-1}^{+1} \Big[\ln \frac{(k_\delta)_{\tilde{\kappa}_{1,\delta}}}{(k_\delta)_{\hat{\kappa}_0}} + k_\delta \ln \frac{\lambda_{1,\delta}(\hat{n}_b + \hat{\kappa}_0)}{\hat{n}_b(\lambda_{1,\delta} + \tilde{\kappa}_{1,\delta})} + \phi_{\text{off},\delta} \Big] + \gamma_{\text{co}} \ln(1 + k_{i,m}) \sum_{\delta=\pm 1} \hat{\eta}_\delta \ln(1 + k_\delta), \tag{6}$$

where $(k)_\kappa = \Gamma(k+\kappa)/\Gamma(\kappa)$, $\lambda_{1,\delta} = \hat{\eta}_\delta \hat{n}_s + \hat{n}_b$, and $\phi_{\text{off},\delta} = \tilde{\kappa}_{1,\delta} \ln[\tilde{\kappa}_{1,\delta}/(\lambda_{1,\delta} + \tilde{\kappa}_{1,\delta})] - \hat{\kappa}_0 \ln[\hat{\kappa}_0/(\hat{n}_b + \hat{\kappa}_0)]$. For fixed adjacent counts $k_{m\pm 1} \geq 0$, $\ell_m(\mathbf{k}_i)$ is strictly increasing ($\Delta_{k_m} \ell_m > 0$) and strictly concave ($\Delta_{k_m}^2 \ell_m < 0$) for all $k_m \triangleq k_{i,m} \geq 0$.

Proof: For fixed $k_{m\pm 1} \geq 0$, the $\delta = \pm 1$ bracketed terms in (6) are independent of k_m, and $C_{\text{adj}} \triangleq \gamma_{\text{co}} \sum_{\delta=\pm 1} \hat{\eta}_\delta \ln(1 + k_{m+\delta}) \geq 0$ is a non-negative constant. Since $\rho_0 > 0$ and $\xi = \hat{\kappa}_0 \hat{\text{SI}}_{\text{tot}} > 0$, $\tilde{\kappa}_{1,0} = \hat{\kappa}_0[1 + \rho_0/(1+\xi)]$ strictly satisfies $\hat{\kappa}_0 < \tilde{\kappa}_{1,0} < \hat{\kappa}_0(1+\rho_0) = \hat{\kappa}_0(\lambda_{1,0}/\hat{n}_b)$. Using $\Gamma(x+1) = x\Gamma(x)$, the first forward difference $\Delta_{k_m} \ell_m(\mathbf{k}_i) = \ell_m(k_m + 1) - \ell_m(k_m)$ is

$$\Delta_{k_m} \ell_m(\mathbf{k}_i) = \ln \left(\frac{k_m + \tilde{\kappa}_{1,0}}{k_m + \hat{\kappa}_0} \right) + \ln \left[\frac{\lambda_{1,0}(\hat{n}_b + \hat{\kappa}_0)}{\hat{n}_b(\lambda_{1,0} + \tilde{\kappa}_{1,0})} \right] + C_{\text{adj}} \ln \left(\frac{k_m + 2}{k_m + 1} \right) > 0, \tag{7}$$

because all three logarithmic terms have arguments strictly exceeding unity. Taking the second forward difference $\Delta_{k_m}^2 \ell_m(\mathbf{k}_i) = \Delta_{k_m} \ell_m(k_m + 1) - \Delta_{k_m} \ell_m(k_m)$ eliminates the constant slope term and yields

$$\Delta_{k_m}^2 \ell_m(\mathbf{k}_i) = \ln \left[1 - \frac{\tilde{\kappa}_{1,0} - \hat{\kappa}_0}{(k_m + \tilde{\kappa}_{1,0})(k_m + 1 + \hat{\kappa}_0)} \right] + C_{\text{adj}} \ln \left[1 - \frac{1}{(k_m + 2)^2} \right] < 0, \tag{8}$$

which holds strictly for all $k_m \geq 0$ since $\tilde{\kappa}_{1,0} > \hat{\kappa}_0$ and $C_{\text{adj}} \geq 0$ (Fig. 2(a)). ∎

To track residual clock offset $\delta\tau_0 \in [0.10, 0.22]$ slots and first-order autoregressive wander $\tilde{\tau}_b = 0.96\tilde{\tau}_{b-1} + w_b$ after Ka-band group–phase leveling, the receiver computes posterior slot probabilities $p_{i,m} = \text{softmax}(\ell_m(\mathbf{k}_i))$ and evaluates the normalized early–late timing error detector (TED):

$$e_{\text{TED},b} = \frac{1}{W_{\text{eff},b}} \sum_{i=1}^{N_{\text{sym}}} w_i \sum_{m=0}^{M-1} p_{i,m} \big(k_{i,m+1} - k_{i,m-1} \big), \tag{9}$$

where $w_i = \max_m p_{i,m}$ and $W_{\text{eff},b} = \sum_{i=1}^{N_{\text{sym}}} w_i \max(K_{i,\mathcal{W}} - 3\hat{n}_b, 0.25)$ normalizes the TED gain to unity ($\partial \mathbb{E}[e_{\text{TED},b}]/\partial \delta\tau_b \approx 1$). A 1D scalar Kalman filter updates the NCO timing shift $\hat{\mu}_d(b) = \hat{\mu}_d(b-1) + K_b e_{\text{TED},b}$ with Riccati gain $K_b = P_{b|b-1}/(P_{b|b-1} + R_b)$, $P_{b|b-1} = 0.96^2 P_{b-1} + Q_b$, and measurement variance $R_b = (\sigma_{\text{TDC}}^2 + P_{b|b-1} + 0.15\hat{n}_b)/\max(W_{\text{eff},b}/10, 1)$ ($\sigma_{\text{TDC}} = \Delta t_{\text{TDC}}/(\sqrt{12} T_{\text{slot}})$), shifting streaming 15.625 ps time-to-digital converter (TDC) timestamps on-the-fly across the 16-slot guard interval without storing full-frame timestamp buffers. After a 2-step pull-in over the 128-symbol CCSDS Attached Sync Marker (ASM), steady-state slot drift drops $11.4\times$ from 0.1545 to 0.0135 slots (Fig. 2(b)).

IV. PERFORMANCE EVALUATION AND DISCUSSION

Five transceiver configurations are evaluated across a Common Random Numbers (CRN) Monte Carlo ensemble at Mars Superior Solar Conjunction ($D = 1.52$ AU, $\alpha_{\text{SEP}} = 2.5^\circ$, 8 seeds × 4,800 symbols = 38,400 symbols / 1,200 blocks for Rate-1/2 $[16, 8, 5]$ Extended Quadratic Residue (QR) soft decoding, plus a 64-epoch / 384,000-symbol / 2,400-superframe ensemble spaced over 512 s $> \tau_{\text{cor}}$ for 960-bit CCSDS Serially Concatenated PPM (SCPPM) [5], confirming 0.761 ± 0.002 μrad RMSE and QR FER 0.0231 ± 0.0014).

In Table II and Fig. 3, Configuration 1 (CCSDS static Poisson [3]) suffers 3.409 μrad pointing RMSE and bunched LLR saturation (FER = 1.000). Configuration 2 (5 kW ground beacon [2]) reduces pointing error to 0.934 μrad (18.78 Mbps), whereas Configuration 3 (hard-switched RF/FSO [9]) mutes the optical link when FER > 0.50. Comparing Configuration 4 (proposed onboard PAT with open-loop timing, 29.72 Mbps) to Configuration 5 (full proposed architecture, 36.97 Mbps, 0.639 bits/photon vs. the 1.308 bits/photon Pierce capacity bound [4]), the 3-slot concave LLR and Kalman timing loop together reduce $[16, 8, 5]$ QR FER by $9.3\times$ ($0.2167 \to 0.0233$) and 960-bit SCPPM FER by $64.2\times$ ($0.1092 \to 0.0017$, $262/2400 \to 4/2400$ frame errors, non-overlapping Clopper–Pearson 95% CIs $[0.0970, 0.1224]$ vs. $[0.0005, 0.0043]$, sustaining 37.78 Mbps).

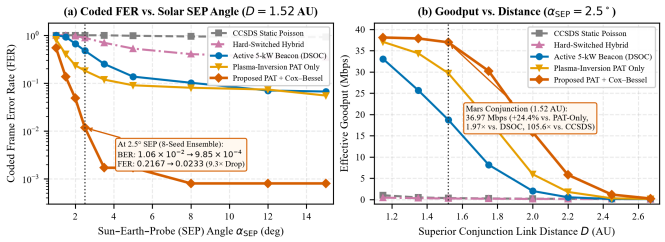


Fig. 3. Multi-baseline CRN sweeps: (a) Coded FER vs. α_{SEP} at $D = 1.52$ AU ($9.3\times$ QR FER reduction over open-loop timing at 2.5°); (b) Effective goodput vs. link distance $D \in [1.15, 2.67]$ AU at $\alpha_{\mathrm{SEP}} = 2.5^\circ$.

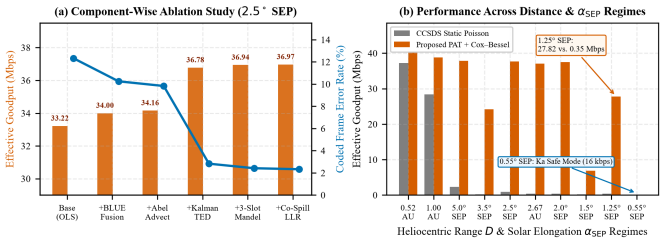


Fig. 4. System validation: (a) Cumulative component ablation from the initial baseline to the full receiver (33.22 → 36.97 Mbps, FER : 12.33% → 2.33%); (b) Orbital and solar-elongation sweep down to $\alpha_{\mathrm{SEP}} = 0.55^\circ$.

Fig. 4(a) details the cumulative component ablation from the initial OLS + fixed-gain TED + top-3 SI baseline (1.131 μrad, 0.1034 slot drift, 33.22 Mbps): adding BLUE fusion (0.879 μrad, 34.00 Mbps), radial Abel advection (0.763 μrad, 34.16 Mbps), 1D Kalman timing (0.0266 slots, 36.78 Mbps), 3-slot Mandel SI (0.0145 slots, 36.94 Mbps), and co-spill LLR damping (0.0135 slots, 36.97 Mbps; paired across the 64 independent 8.0 s epochs, df $=$ 63, QR ΔFER $= -0.00092 \pm 0.00028$, t-test $p = 0.0018$, Wilcoxon $p = 0.0024$) yields strictly monotonic gains. On an Intel Core 7 150U CPU (64-sub-block elastic FIFO), lookup-table demodulation, TED, and 120 QR decoders execute in 23.83 μs per 25.60 μs sub-block (25.12 μs 99.9th-percentile; 24.60 μs mean / 25.44 μs 99.9th-percentile with 6-iteration max-log-MAP SCPPM, 0 buffer overruns).

Across $\pm 15\%$ Leblanc profile errors, $\pm 20\%$ solar-wind velocity transients, and $\pm 50\%$ Rytov prior perturbations, effective goodput varies by $<$ 0.28 Mbps. Because scalar plane-of-sky OD correction leaves a 0.20 μrad out-of-plane ephemeris floor, embedding X/Ka plasma states directly into a 6-state orbit determination filter is a promising direction for future work. In Fig. 4(b), optical lock holds down to $\alpha_{\mathrm{SEP}} = 1.25^\circ$ ($R_0 = 4.69\, R_\odot$, 27.82 Mbps), below which coronal mass ejections or solar limb grazing ($\alpha_{\mathrm{SEP}} \le 0.55^\circ$) trigger automatic handover to the 16 kbps Ka-band telemetry link.

V. Conclusion

This letter presented a causal two-node optical–RF transceiver for deep-space links near Superior Solar Conjunction. By combining onboard dual-band X/Ka BLUE plasma inversion and radial Abel advection with a ground 3-slot strictly concave soft demodulator (Theorem 1) and 1D Kalman timing loop, the transceiver achieves 0.763 μrad pointing RMSE, $11.4\times$ lower slot drift, and 36.97 Mbps goodput at 1.52 AU without an uplink laser beacon.

References

[1] D. M. Boroson *et al.*, "Overview and results of the Lunar Laser Communication Demonstration," in *Proc. SPIE*, vol. 8971, Mar. 2014, Art. no. 89710S, doi: 10.1117/12.2045508.

[2] H. Hemmati, A. Biswas, and I. B. Djordjevic, "Deep-space optical communications: Future perspectives and applications," *Proc. IEEE*, vol. 99, no. 11, pp. 2020–2039, Nov. 2011, doi: 10.1109/JPROC.2011.2160609.

[3] *Optical Communications Physical Layer*, CCSDS Blue Book 141.0-B-1, Consult. Comm. Space Data Syst., Washington, DC, USA, 2019.

[4] J. R. Pierce, "Optical channels: Practical limits with photon counting," *IEEE Trans. Commun.*, vol. 26, no. 12, pp. 1819–1821, Dec. 1978, doi: 10.1109/TCOM.1978.1094043.

[5] B. Moision and J. Hamkins, "Low-complexity serially-concatenated coding for the deep space optical channel," in *Proc. IEEE ISIT*, Jun. 2003, p. 269, doi: 10.1109/ISIT.2003.1228283.

[6] E. E. Wollman *et al.*, "Kilopixel array of superconducting nanowire single-photon detectors," *Opt. Express*, vol. 27, no. 24, pp. 35279–35289, Nov. 2019, doi: 10.1364/OE.27.035279.

[7] Y. Leblanc, G. A. Dulk, and J.-L. Bougeret, "Tracing the electron density from the corona to 1 AU," *Solar Phys.*, vol. 183, no. 1, pp. 165–180, Nov. 1998, doi: 10.1023/A:1005049730506.

[8] D. D. Morabito, "Solar corona-induced fluctuations on spacecraft signal amplitude observed during solar superior conjunctions of the Cassini spacecraft," *Radio Sci.*, vol. 42, no. 3, Art. no. RS3002, 2007, doi: 10.1029/2005RS003425.

[9] M. Usman, H.-C. Yang, and M.-S. Alouini, "Practical switching-based hybrid FSO/RF transmission and its performance analysis," *IEEE Photon. J.*, vol. 6, no. 5, pp. 1–13, Oct. 2014, doi: 10.1109/JPHOT.2014.2352629.

[10] I. I. Shapiro, "Fourth test of general relativity," *Phys. Rev. Lett.*, vol. 13, no. 26, pp. 789–791, Dec. 1964, doi: 10.1103/PhysRevLett.13.789.

[11] H. Kaushal and G. Kaddoum, "Optical communication in space: Challenges and mitigation techniques," *IEEE Commun. Surveys Tuts.*, vol. 19, no. 1, pp. 57–96, 1st Quart., 2017, doi: 10.1109/COMST.2016.2603518.

[12] B. Bertotti, L. Iess, and P. Tortora, "A test of general relativity using radio links with the Cassini spacecraft," *Nature*, vol. 425, pp. 374–376, Sep. 2003, doi: 10.1038/nature01997.

[13] H. C. van de Hulst, "The electron density of the solar corona," *Bull. Astron. Inst. Neth.*, vol. 11, pp. 135–150, Feb. 1950.

[14] R. Rogalin and M. Srinivasan, "Maximum likelihood synchronization for pulse position modulation with inter-symbol guard times," in *Proc. IEEE GLOBECOM*, Dec. 2016, pp. 1–6, doi: 10.1109/GLOCOM.2016.7842177.

[15] M. A. Al-Habash, L. C. Andrews, and R. L. Phillips, "Mathematical model for the irradiance probability density function of a laser beam propagating through turbulent media," *Opt. Eng.*, vol. 40, no. 8, pp. 1554–1562, Aug. 2001, doi: 10.1117/1.1386641.